# Fabrication and high-resolution electron microscopy study of FePt L1 0 /A1 graded exchange spring media

**ARTICLE** *in* PHYSICA STATUS SOLIDI (A) · JULY 2013

Impact Factor: 1.21 · DOI: 10.1002/pssa.201228731



**8 AUTHORS**, INCLUDING:

Jehyun Lee
Samsung Advanced Institute of Technology
**952** PUBLICATIONS **6,997** CITATIONS
SEE PROFILE

Vasileios Alexandrakis
Ruhr-Universität Bochum
**17** PUBLICATIONS **261** CITATIONS
SEE PROFILE

Thanassis Speliotis
National Center for Scientific Research De…
**81** PUBLICATIONS **395** CITATIONS
SEE PROFILE

Dimitris Niarchos
National Center for Scientific Research De…
**448** PUBLICATIONS **5,105** CITATIONS
SEE PROFILE

WILEY ONLINE LIBRARY EarlyView publication on wileyonlinelibrary.com
(issue and page numbers not yet assigned;
citable using Digital Object Identifier – **DOI**)

Phys. Status Solidi A, 1–6 (2013) / **DOI** 10.1002/pssa.201228731

physica status solidi pss a
www.pss-a.com
*applications and materials science*

**Part of Topical Section on**
**Terabit Recording and Magnetic Nanostructures**

# Fabrication and high-resolution electron microscopy study of FePt $L1_0$/A1 graded exchange spring media

**Jehyun Lee[1,3†], Barbara Dymerska[1], Josef Fidler[*,1], Vasilis Alexandrakis[2], Thanassis Speliotis[2], Dimitris Niarchos[2], Peter Pongratz[1], and Dieter Suess[1]**

[1] Institute of Solid State Physics, Vienna University of Technology, Wiedner Hauptstrasse 8-10, 1040 Vienna, Austria
[2] IMS, NCSR Demokritos, Aghia Paraskevi, Attikis, Athens 15310, Greece

Received 23 October 2012, revised 14 March 2013, accepted 18 March 2013
Published online 25 April 2013

**Keywords** exchange spring media, FePt, HRTEM, magnetic recording, transmission electron microscopy

[*] Corresponding author: e-mail josef.fidler@tuwien.ac.at, Phone: +43 1 58801 13729, Fax: +43 1 58801 13899
[†] Present address: Department of Advanced Materials, Samsung Advanced Institute of Technology, 446-712 Yongin-si, Republic of Korea.

We have prepared FePt $L1_0$/A1 exchange spring graded media by controlling deposition temperature. The performance of the media was determined by the deposition conditions, particularly the cooling rate. By varying the deposition conditions a coercivity of 4.0 kOe was achieved without loss in remanent magnetization, the value corresponds to 88% reduction compared with that of FePt $L1_0$ single phase (32.2 kOe). High-resolution transmission electron microscopy (HRTEM) investigations have revealed that this drastic coercivity reduction originates from the unique microstructure of the specimens: coexistence of the $L1_0$ and A1 phases at the interphase boundary. In this region the two phases are dispersed one into another like inclusions in a matrix. Finally, the role of the complicated phase boundary on switching field reduction was discussed using micromagnetic simulations.

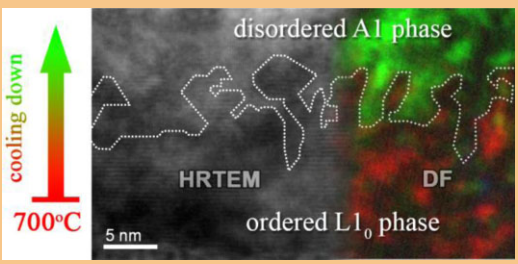




**1 Introduction** In recent developments of advanced recording media, exchange spring media based on FePt $L1_0$ ordered phase has been the most promising candidate to achieve the recording density beyond 1 Tbit in$^{-2}$ with high thermal stability [1, 2]. The performance of the FePt $L1_0$ phase-based exchange spring media is usually determined by the pinning field between the recording layer, FePt $L1_0$ ordered hard phase, and the reversal domain nucleation layer, such as [Co/Pt] multilayer, CoPt $L1_0$ phase, Fe and FePt A1 disordered soft phase [3–7]. For reduction of the pinning field, the theory suggests to insert many intermediate layers with a proper crystalline anisotropy between the two layers (stacked graded media) [8–10]. Previously, using micromagnetic simulations we have shown that the pinning field is also able to be decreased if the interface between the phases is very rough (phase-graded media) [11]. In that case the reversal domain propagates into the hard phase through the sharp wedges of the hard phase inside the soft phase. In this paper the deposition temperature control was used for introducing a rough interphase boundary, assuming the gradual secondary phase (FePt A1 phase) formation under gradually decreasing deposition temperature [12]. In this article we present the performance of the realized phase-graded media prepared with temperature control. The microstructure was investigated using electron microscopy, then implemented into finite-element (FE) models in order to study the contribution of the microstructure to the magnetization behaviors.

**2 Experimental results** FePt layers were deposited onto (001) textured MgO substrate using DC magnetron sputtering. First, 11.5 nm of FePt was deposited at 700 °C. By X-ray diffraction spectra (XRD) and transmission electron microscopy (TEM) the microstructure of the specimen was verified as a $L1_0$ phase [13]. It is known that the crystalline structure of the FePt film on MgO (001) substrate is determined by deposition temperature, and 700 °C is a suitable temperature for $L1_0$ phase formation [5, 14, 15]. Subsequently, the second FePt layer was deposited on top of the $L1_0$ phase while the substrate was being cooled down to the given final temperature ($T_{final}$). In this paper this secondary layer is named as a "graded layer" because the degree of ordering is expected to be graded. The thickness of graded layer ($t_{graded}$) and $T_{final}$ were varied in four cases. The hysteresis loops were measured by a typical vibrating sample magnetometry (VSM), the results are presented in Fig. 1. For all specimens the coercivity ($H_C$) in kOe and remanent magnetization ($M_r$) normalized to saturation magnetization ($M_S$) are summarized in Table 1. These data are compared with those of the 11.5-nm thick FePt $L1_0$ single-phase layer. Except for the specimen A, which has only 2.31 nm of graded layer, the coercivities were drastically reduced by additional deposition of the graded layer. The coercivity reduction of the samples B and C were 87.6% and 70.1%, respectively, whereas the remanent magnetizations were hardly affected. Severe reduction of the remanent magnetization was observed only for the sample D, with the largest coercivity drop as well as with a big change in the shape of the hysteresis loop. Such behavior is supposed to be due to the soft phase thick enough to release the spins from the perpendicular alignment at the remanent state [16]. In order to elucidate the origin of the dramatic change in the magnetic properties, we have investigated the microstructures of the specimens.

**3 Microstructural analysis** The microstructure of the FePt graded media was studied using FEI Quanta 200 field emission gun scanning electron microscopy (FEG SEM) and FEI TECNAI F20 TEM. The TEM specimens were prepared by the conventional method using SiC paper and diamond sheets, followed by Ar ion milling using a Precision Ion Polishing System (PIPS). The acceleration voltage during PIPS process was reduced to 1.0 keV at the final stage to prevent possible damages caused by ion beam. Figure 2a shows the plan view image of the FePt films. Strongly faceted islands of FePt grains are observed. The island facets along the [100] and [010] directions occur most frequently in specimen A, which has the smallest graded layer thickness of 2.3 nm and the highest $T_{final}$ of 600 °C. The tendency of the facet alignment weakens in other specimens, which have a thicker graded layer and lower $T_{final}$, consequently sample D has very few facets remaining [17].

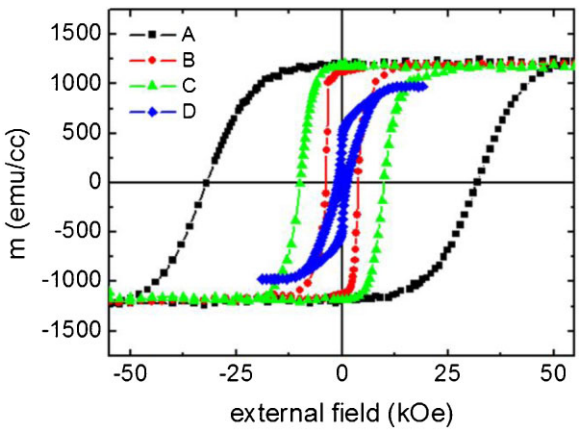


**Figure 1** Hysteresis loops of the FePt graded media.

**Table 1** Thickness ($t_{graded}$), final temperature ($T_{final}$) and cooling rate of the graded layer deposited on top of 11.5 nm FePt $L1_0$ phase layer at 700 °C, with the $H_C$ of the FePt graded media. The $t_{graded}$ are not measured values, but expected ones by the deposition rate and the sputtering time.

| specimen no. | $t_{graded}$ (nm) | $T_{final}$ (°C) | cooling rate (°C nm$^{-1}$) | $H_C$ (kOe) | $M_r$ ($M_S$) |
|---|---|---|---|---|---|
| FePt $L1_0$ | 0 | 700 | – | 33.2 | 0.98 |
| A | 2.31 | 600 | 43.5 | 32.1 | 0.96 |
| B | 11.1 | 600 | 9.01 | 4.00 | 0.94 |
| C | 10.0 | 450 | 25.0 | 9.62 | 0.98 |
| D | 37.5 | 262 | 11.7 | 1.25 | 0.45 |

Selective-area diffraction patterns (SADP) were obtained for all the graded media specimens. The one from the specimen D is shown in Fig. 2b as a representative. A complicated double-diffraction spot pattern is observed, which is typically found in incommensurate or commensurate modulated structures [18]. All of the diffraction spots include strong and weak ones located in two-dimensional square patterns with a lattice constant of $2.32 \pm 0.23$ nm. This value equals 11 times of the $d$-spacing of MgO (200), 0.211 nm and 12 times the $d$-spacing of FePt $L1_0$ (200), 0.193 nm or FePt A1 (200), 0.191 nm [19]. The spot patterns from the $L1_0$ phase and the A1 phase were not distinguishable due to the very small difference between their (002) $d$-spacings. The double-diffraction pattern reveals that the crystal structures of FePt film is undistorted and parallel to that of the MgO substrate.

The distribution of the $L1_0$ and A1 phases is clearly shown in the cross-sectional high-resolution transmission electron microscopy (HRTEM) images accompanied by their SADPs (Fig. 3). Since FePt $L1_0$ phase has a superlattice structure of alternating Fe and Pt monoatomic layers, the $L1_0$ phase is represented as repeated stripes perpendicular to the $c$-axis in HRTEM images, whereas the A1 phase is displayed as fourfold symmetrically arranged dots in a square manner.

The HRTEM images in Fig. 3 clearly show the two phases. The phase distributions are recognized by the patterns expected by the image simulations, and the interphase boundaries between them are marked with the dotted lines [20].

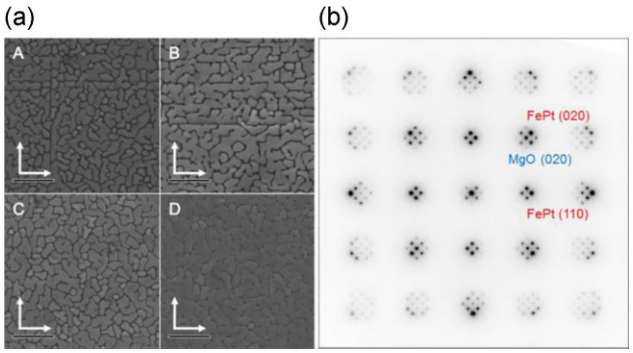


**Figure 2** (a) Scanning electron microscopy (SEM) images of the FePt graded media (scale bars: 500 nm). (b) Selective-area diffraction patterns (SADP) of the specimen D. The arrows indicate the [100] and [010] directions of the MgO substrate. The spots marked with red and blue circles correspond to the ones from FePt film and MgO substrate.

The coexistence of the $L1_0$ and A1 phases is also verified by the cross-sectional SADP images. The diffraction patterns from all specimens are identical, made up of the diffraction patterns of MgO substrate, FePt $L1_0$ phase and FePt A1 phase. The diffraction spots of the A1 phase are mostly overlapped with the ones from the $L1_0$ phase, where the spots correspond to (200) and (002).

It should be noted that the interphase boundary has a complicated profiles. Mixture of the $L1_0$ and A1 phases are experimentally observed in statically annealed specimens during the phase transition from one phase to the other, of which the annealing temperature is in the range of the phase transition [21, 22]. The experiments considering $L1_0$ formation by means of thermal treatment have revealed that inside of an A1 phase matrix the secondary phase is formed, which grows up to the point that the entire film is a single phase $L1_0$ [23].

Our specimens were deposited at decreasing temperatures, therefore the nuclei of the A1 phase developed on the $L1_0$ phase film would have grown along the thickness. The coexistence of the two phases would have been maintained if the cooling rate was small enough. The rough interphase structure was as expected from the first-principles calculations [24].

In the specimen D, which has the most complicated interphase boundary, the $L1_0$ phase inclusions are surrounded by the A1 phase matrix, and vice versa. However, the thickness of the interphase boundary is smaller than the intended one, $t_{graded}$. According to the results obtained from the $Fe_{51}Pt_{49}$ alloy prepared at a static temperature, a small portion of $L1_0$ phase is still formed even at 300 °C [15], whereas our results show that the phase transition is completed at temperatures higher than 600 °C (specimen A and B). Considering the varied $L1_0$ formation temperature in different conditions, the changed residual stress on the depositing layer could be one reason [14, 25], but the detailed mechanism of the early phase transition is not yet clear.

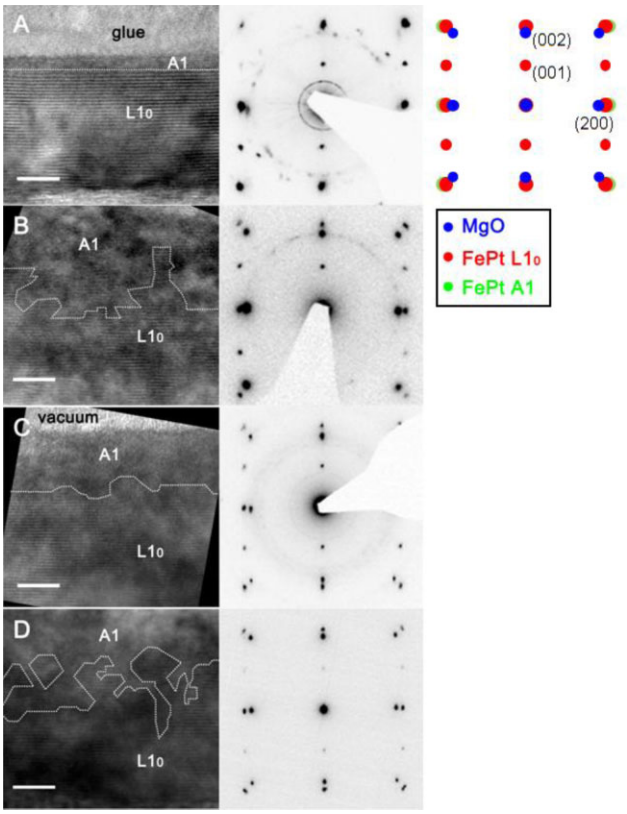


**Figure 3** High-resolution transmission electron microscopy (HRTEM) images (left) and the corresponding selected-area diffraction patterns (SADPs; right). Simulated diffraction patterns are included for comparison (right). The interphase boundaries between $L1_0$ ordered phase and A1 disordered phase are marked with dotted lines. The scale bars correspond to 5 nm. Diffraction rings are found in the SADPs. Judging from the radius of the rings, the rings are supposed to result from the ion damaged part of the specimen, mostly MgO substrate.

Nevertheless, it is obvious that the interphase boundary roughness is highly dependent on the cooling rate. As an example, the interphase boundary of the specimen C (cooling rate = 25.0 °C $nm^{-1}$) is much flatter than that of specimen B (cooling rate = 9.01 °C $nm^{-1}$). Likewise, the specimens with similar cooling rate (B and D) have similar roughness of the interphase boundary. The efficient coercivity reduction was achieved in these specimens as well. The rough interphase boundary between the two phases is double checked by bright-field (BF) and dark-field (DF) images of the specimen D as shown in Fig. 4. The DF images are taken from the MgO (002), FePt $L1_0$ (001), and FePt A1 (002) spots indicated in Fig. 3.

Please note that the boundary between the FePt $L1_0$ phase (Fig. 4c) and FePt A1 phase (Fig. 4d) is quite rough compared with the one between the MgO substrate (Fig. 4b) and FePt $L1_0$ phase (Fig. 4c). For clearer understanding, the DF images are overlapped after coloring in Fig. 4e. The DF images prove the findings from the HRTEM images in Fig. 3.

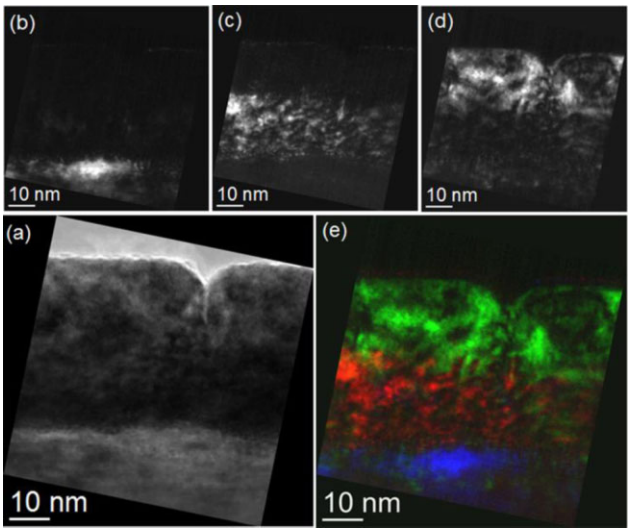


**Figure 4** (a) Bright-field (BF) image and dark-field (DF) images for (b) MgO (002), (c) FePt $L1_0$ (001), and (d) FePt $L1_0$ (002) + A1 (002). (e) The overlapped dark-field images.

**4 Micromagnetic simulations** When a saturated bit of exchange graded media is reversed by a uniform external magnetic field, the switching process is performed by domain-wall propagation [1]. In our FePt $L1_0$/A1 graded media, domain reversal is initiated at the top where the A1 phase is dominant. Afterwards, the domain wall propagates through the graded layer to magnetize the $L1_0$ phase at the bottom. If the medium is a bilayer with a sharp flat interphase boundary the switching field would be determined by the pinning field between the phases, which is proportional to the difference of the uniaxial anisotropies [8, 10],

$$H_{\text{pin}} = \frac{2\left(K_{\text{U,L10}} - K_{\text{U,A1}}\right)}{\left(\sqrt{J_{\text{S,L10}}} + \sqrt{J_{\text{S,A1}}}\right)^2} = 24.1\,\text{kOe}. \quad (1)$$

Here, the crystalline anisotropy $K_{\text{U}}$ and saturation polarization $J_{\text{S}}$ of the two phases are $K_{\text{U,L10}} = 5\,\text{MJ m}^{-3}$, $K_{\text{U,A1}} = 0.1\,\text{MJ m}^{-3}$, $J_{\text{S,L10}} = 1.58\,\text{T}$, and $J_{\text{S,A1}} = 1\,\text{T}$ [26]. Please note that the Eq. (1) works only for a special case that the exchange coefficient of the two phases are same [8, 10]. In this study the exchange coefficients $A_{\text{L10}}$ and $A_{\text{A1}}$ are supposed to have same value, $10\,\text{pJ m}^{-1}$. From the thermal-fluctuation-induced deviation between the switching fields of FePt $L1_0$ single phase obtained experimentally (32.2 kOe) and theoretically ($2K_{\text{U,L10}}/J_{\text{S,L10}} = 79.5\,\text{kOe}$), the experimental switching field of the FePt $L1_0$/A1 bilayer with a sharp flat interphase boundary is supposed to be 9.76 kOe [27]. The value is very close to the switching field of the specimen C (9.36 kOe), which has an adequately thick graded layer and small interphase boundary roughness. It should be noted that the specimens with rough interphase boundary (B and D) have much smaller switching fields than the specimen C.

In order to understand how the rough interphase boundaries reduce the coercivity and to find out the optimum structure of the FePt $L1_0$/A1 graded media, FE micromagnetic simulations were performed using FEMME neglecting thermal fluctuation [28]. The FE models of the graded media were prepared by building 10 nm × 10 nm × 25 nm bit models consisting of 1 nm × 1 nm × 1 nm discretization cells. To each cell, proper material properties of one of the two possible phases were assigned [11]. For the purpose of reflecting the microstructure, the bottom and the top parts are defined as only $L1_0$ and A1 phases, respectively, whereas the interphase boundary is a mixture of the two phases, as observed in the cross-sectional TEM study. The interphase boundary thickness was varied from 3 to 21 nm, where the portion of the two phases in this region is also varied according to linear, quadratic, and logistic distributions. Following the microstructural findings, the $L1_0$ and A1 phases are randomly assigned at the interphase boundary in agreement with the occurrence probability obtained by the distribution functions. Figure 5a shows the FE model of the FePt $L1_0$/A1 graded media, with linearly distributed 18 nm interphase boundary.

In Fig. 5b, it is found that much lower switching fields than the value expected from the Eq. (1) are obtained at various conditions: the magnetization procedures of our FePt $L1_0$/A1 graded media is as follows. When the domain wall inside A1 phase moving toward the interphase boundary meets the $L1_0$ phase inclusions, an additional external magnetic field is required to reverse the hard-phase materials. However, the required field is much weaker than the case of a traditional bilayer that allows the penetration of the domain wall only from the flat interface between the two phases, because the domain wall surrounds the small portion of the hard phase at the rough interphase boundary. In this procedure the additionally applied field is stored in the domain wall as a form of the narrower domain-wall width. The compressed domain wall with higher energy is

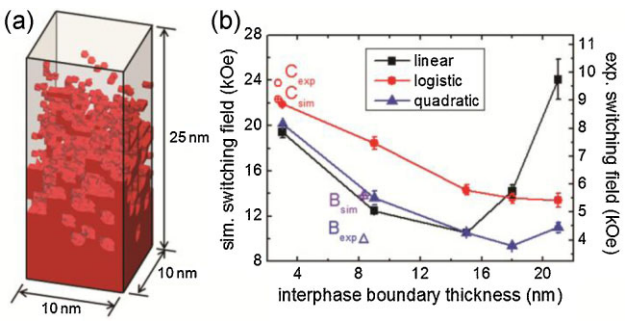


**Figure 5** (a) An example of the finite-element model of the FePt $L1_0$/A1 graded media, with a linearly distributed 18-nm thick interphase boundary. (b) Switching fields of the media as a function of the interphase boundary thickness, for various phase dispersions at the phase boundary. The experimental results and the simulated ones from the directly imported microstructures of the specimen B and C are marked for comparison.

easier to penetrate into the hard phase [29]. The procedure of domain-wall compression and depinning was explained in detail by Dobin, Kronmüller, Goll and coworkers [30–32]. Once the domain wall is penetrated into a branch of the $L1_0$ phase, no further external field is required to magnetize the whole hard phase. As a result, as revealed in the simulation results in Fig. 5b, the switching field of the graded layer was reduced up to 9.36 kOe for the case of quadratic distributions of the A1 phase with 18 nm of interphase boundary thickness. The switching field is only 33.4% of the FePt $L1_0$/A1 bilayer with a flat sharp interphase boundary between them, as well as only 11.8% of the FePt $L1_0$ single-phase media.

The simulations were performed on the models directly imported from the HRTEM images of the specimens B and C, the results are plotted on Fig. 5b with comparisons with the experimental ones. From the analysis of the HRTEM images the specimen B is found to have a quadratic interphase boundary profile with a boundary thickness of 8.3 nm, and the specimen C has a 2.7-nm thick logistic interphase boundary. There is a deviation in the results from the specimen B where C shows a good agreement between the experiment and the simulation. The deviation is supposed to result from inevitable inaccurate HRTEM image analysis, particularly for the specimens with a very rough interface. Since the TEM specimen has a thickness of at least tens of nanometers, the $L1_0$ and the A1 phases are distributed along the thickness direction. The thickness-directional phase distribution must have influenced the lattice fringes shown in HRTEM image, therefore the phase boundary could not be drawn accurately. From the comparison of the switching fields of the specimen B, it seems that the thickness of the interphase boundary is underestimated by 9 nm. The numerical approach based on the TEM observation is explained in more detail in another paper [33].

**5 Conclusions** We have produced the FePt $L1_0$/A1 graded media by magnetron sputtering at controlled temperatures, for which the coercivity was reduced up to 88% without a decline in remanent magnetization. The better performance was achieved by a lower cooling rate, therefore the interphase boundary is thicker. The electron microscopy microstructure investigations have revealed that the FePt $L1_0$ and A1 phases coexist with very complicated boundaries between them, the phases are dispersed into the other. From the micromagnetic simulations it is found that the phase distribution efficiently reduces the pinning field between the phases by transferring the external field into domain-wall energy.

**Acknowledgements** This work was supported by the EU FP7 project TERAMAGSTOR (ICT No. 2240001). All TEM investigations were carried out using facilities at the University Service Centre for Transmission Electron Microscopy, Vienna University of Technology, Austria.

## References

[1] D. Suess, T. Schrefl, S. Fahler, M. Kirschner, G. Hrkac, F. Dorfbauer, and J. Fidler, Appl. Phys. Lett. **87**, 012504 (2005).
[2] R. H. Victora and S. Xiao, IEEE Trans. Magn. **41**, 537–542 (2005).
[3] F. Wang, X.-H. Xu, Y. Liang, J. Zhang, and J. Zhang, Mater. Chem. Phys. **126**, 843–846 (2011).
[4] D. Goll, A. Breitling, L. Gu, P. A. van Aken, and W. Sigle, J. Appl. Phys. **104**, 083903–083904 (2008).
[5] V. Alexandrakis, D. Niarchos, K. Mergia, J. Lee, J. Fidler, and I. Panagiotopoulos, J. Appl. Phys. **107**, 013903 (2010).
[6] D. Makarov, J. Lee, C. Brombacher, C. Schubert, M. Fuger, D. Suess, J. Fidler, and M. Albrecht, Appl. Phys. Lett. **96**, 062501 (2010).
[7] K. K. M. Pandey, J. S. Chen, and G. M. Chow, IEEE Trans. Magn. **46**, 1955–1958 (2010).
[8] H. Kronmüller and M. Fähnle, Micromagnetism and the Microstructure of Ferromagnetic Solids (Cambridge University Press, Cambridge, 2003).
[9] D. Suess, Appl. Phys. Lett. **89**, 113105 (2006).
[10] H. Kronmüller and D. Goll, Phys. B: Condens. Matter **319**, 122–126 (2002).
[11] J. Lee, V. Alexandrakis, M. Fuger, B. Dymerska, D. Suess, D. Niarchos, and J. Fidler, Appl. Phys. Lett. **98**, 222501 (2011).
[12] W. S. Tong, J. M. Rickman, and K. Barmak, J. Chem. Phys. **114**, 915–922 (2001).
[13] V. Alexandrakis, T. Speliotis, E. Manios, D. Niarchos, J. Fidler, J. Lee, and G. Varvaro, J. Appl. Phys. **109**, 07B729 (2011).
[14] S. N. Hsiao, F. T. Yuan, H. W. Chang, H. W. Huang, S. K. Chen, and H. Y. Lee, Appl. Phys. Lett. **94**, 232505 (2009).
[15] S. N. Hsiao, S. K. Chen, T. S. Chin, Y. W. Hsu, H. W. Huang, F. T. Yuan, H. Y. Lee, and W. M. Liao, J. Magn. Magn. Mater. **321**, 2459–2466 (2009).
[16] D. Suess, J. Magn. Magn. Mater. **308**, 183–197 (2007).
[17] T. Shima, K. Takanashi, Y. K. Takahashi, and K. Hono, Appl. Phys. Lett. **81**, 1050–1052 (2002).
[18] J. C. Jiang, Appl. Phys. Lett. **90**, 051904 (2007).
[19] JCPDS-International_Center_of_Diffraction_Data (1999).
[20] J. M. Zuo, Web Electron Microscopy Applications Software (WebEMAPS), http://emaps.mrl.uiuc.edu/emaps.asp, University of Illinois.
[21] R. A. Ristau, K. Barmak, L. H. Lewis, K. R. Coffey, and J. K. Howard, J. Appl. Phys. **86**, 4527–4533 (1999).
[22] F. E. Spada, F. T. Parker, C. L. Platt, and J. K. Howard, J. Appl. Phys. **94**, 5123–5134 (2003).
[23] N. Murayama, S. Soeya, Y. Takahashi, and M. Futamoto, J. Magn. Magn. Mater. **320**, 3057–3059 (2008).
[24] Y. Misumi, S. Masatsuji, R. Sahara, S. Ishii, and K. Ohno, J. Chem. Phys. **128**, 234702–234705 (2008).
[25] J. K. Mei, F. T. Yuan, W. M. Liao, Y. D. Yao, H. M. Lin, J. H. Hsu, and H. Y. Lee, IEEE Trans. Magn. **47**, 3629–3632 (2011).
[26] J. Fidler, P. Speckmayer, T. Schrefl, and D. Suess, J. Appl. Phys. **97**, 10E508 (2005).
[27] D. Suess, L. Breth, J. Lee, M. Fuger, C. Vogler, F. Bruckner, B. Bergmair, T. Huber, J. Fidler, and T. Schrefl, Phys. Rev. B **84**, 224421 (2011).

[28] T. Schrefl and J. Fidler, J. Magn. Magn. Mater. **111**, 105–114 (1992).
[29] A. Y. Dobin and H. J. Richter, Appl. Phys. Lett. **89**, 062512–062513 (2006).
[30] A. Y. Dobin and H. J. Richter, J. Appl. Phys. **101**, 09K108 (2007).
[31] H. Kronmüller and D. Goll, J. Iron Steel Res. Int. **13** (Suppl. 1), 39–47 (2006).
[32] H. Kronmüller and D. Goll, Phys. B: Condens. Matter **403**, 237–241 (2008).
[33] B. Dymerska, J. Lee, J. Fidler, and D. Suess, J. Phys. D, Appl. Phys. **45**, 495001 (2012).

 